

Document downloaded from:

<http://hdl.handle.net/10251/81699>

This paper must be cited as:

Escolástico Rozalén, S.; Kjolseth, C.; Serra Alfaro, JM. (2016). Catalytic activation of ceramic H<sub>2</sub> membranes for CMR processes. *Journal of Membrane Science*. 517:57-63. doi:j.memsci.2016.06.017.



The final publication is available at

<http://doi.org/10.1016/j.memsci.2016.06.017>

Copyright Elsevier

Additional Information

**Catalytic activation of ceramic H<sub>2</sub> membranes for CMR processes**

S. Escolástico<sup>a</sup>, C. Kjølseth<sup>b</sup> and J. M. Serra<sup>a,\*</sup>

<sup>a</sup> *Instituto de Tecnología Química (Universidad Politécnica de Valencia - Consejo Superior de Investigaciones Científicas) Avenida de los Naranjos s/n.46022 Valencia, Spain.*

<sup>b</sup> *Coorstek Membrane Sciences, Forskningsparken, Gaustadalleen 21, NO-0349 Oslo, Norway*

\* *corresponding author: jmserra@itq.upv.es*

**Abstract**

The application of catalytic membrane reactors can overcome some of the disadvantages that reactions for the direct conversion of methane to fuels and petrochemicals present. Hydrogen separation membranes can shift the reaction equilibrium by hydrogen removal, improving the separation, selectivity and yield of the reactions. La<sub>5.5</sub>WO<sub>11.25-δ</sub>/La<sub>0.87</sub>Sr<sub>0.13</sub>CrO<sub>3-δ</sub> (LWO/LSC) based membranes present a high H<sub>2</sub> flux within the temperature range where CMR can be applied. However, the catalytic activity of the material is very low and it has to be improved. This work presents the development of different catalytic layers based on LSC material and the study of their influence on the H<sub>2</sub> flux obtained by using 60/40-LWO/LSC membranes. Membranes coated with porous layer made of Ni-infiltrated La<sub>0.75</sub>Ce<sub>0.1</sub>Sr<sub>0.15</sub>CrO<sub>3-δ</sub> exhibited the best permeation flux but still 20% lower than the one reached using Pt layers. Stability of the catalytic layers is also evaluated under H<sub>2</sub> permeation conditions and under high steam content methane.

## 1. Introduction

The direct conversion of methane to fuels and petrochemicals represents a major challenge. Steam reforming of light hydrocarbons is an industrially important chemical reaction and a key step for producing hydrogen and syngas for ammonia and methanol production, hydrocracking, Fischer-Tropsch synthesis and other important processes in the oil refining and petrochemical industries [1, 2]. Industrial fixed-bed steam reformers suffer however from several problems which seriously affect their operation and performance [3]. These problems comprise low catalyst effectiveness, low heat transfer rates, large temperature gradients and thermodynamic equilibrium constraints. In the last years, the catalytic conversion of methane to aromatics via non-oxidative routes has attracted significant attention. However, this reaction presents very low equilibrium conversions and benzene yields of only  $\sim 7\%$  at the required temperature (950 K) [4].

The integration of this kind of reactions in catalytic membrane reactors (CMR) may allow the process efficiency to be substantially increased. The reaction equilibrium can be shifted by controlled hydrogen removal with the consequent enhancement of separation, selectivity and yield of these reactions [5, 6]. Dense mixed-conducting ceramic membranes are one of the typical inorganic membranes for CMR, specifically, mixed proton electron conducting membranes which present an important hydrogen permeability and catalytic activity at high temperatures [7, 8]. Several ceramic membranes have been tested for water gas shift reaction at high temperature (700-900 °C) and the reported results are promising [9, 10].

Despite the advantages of these membranes,  $H_2$  fluxes obtained up to date are still low for their short-term industrial application. Aiming to improve the  $H_2$  flux, research has been recently focused in the development of dual phase composites, materials formed by two phases, one electron conducting phase and another phase mainly proton conducting. With this strategy, an important improvement of the  $H_2$  flux and stability has been obtained as compared with the single constituent materials. It is noteworthy the significant  $H_2$  fluxes obtained with several cer-mets as Ni-BaCe<sub>0.9</sub>Y<sub>0.1</sub>O<sub>3- $\delta$</sub>  [11], Ni-BaZr<sub>0.1</sub>Ce<sub>0.7</sub>Y<sub>0.2</sub>O<sub>3- $\delta$</sub>  [12] and Ni-BaCe<sub>0.85</sub>Tb<sub>0.05</sub>Zr<sub>0.1</sub>O<sub>3- $\delta$</sub>  [13]. As well as the cer-cers based on BaCeO<sub>3- $\delta$</sub>  or BaCe<sub>1-x</sub>Zr<sub>x</sub>O<sub>3- $\delta$</sub>  based materials as protonic phase and doped ceria as electronic phase [14, 15].

Among the reported dual phase composites, La<sub>5.5</sub>WO<sub>11.25- $\delta$</sub> /La<sub>0.87</sub>Sr<sub>0.13</sub>CrO<sub>3- $\delta$</sub>  (LWO/LSC) based cer-cers present an excellent  $H_2$  flux permeation [16, 17] (which comprises the  $H_2$  flux due to proton transport through the membrane in addition to the  $H_2$  produced by water splitting and concomitant oxide-ion transport) and stability in different atmospheres. Despite the high  $H_2$  flux obtained with this material, it presents a poor catalytic activity toward  $H_2$  exchange [16]. For this reason, a development of a catalytic layer for the improvement of the surface kinetics is mandatory in order to apply this material in CMR.

This strategy has been widely employed for oxygen permeable membranes based on mixed ionic electronic conductors.[18-21] Regarding surface kinetics improvement in H<sub>2</sub> permeable membranes, the use of Pt as catalytic layer is the most reported for different materials as cerates [22], tungstates [23] and dual phase composites [14, 24, 25]. Ni and Pd particles were also employed for the coating of a BaCe<sub>0.85</sub>Tb<sub>0.05</sub>Co<sub>0.1</sub>O<sub>3-δ</sub> perovskite hollow fibre membrane obtaining a significant H<sub>2</sub> flux improvement [26].

The aim of this work is the synthesis and development of different catalytic coatings layers for the mixed protonic-electronic 60/40-LWO/LSC (60:40 in volume) composite with the purpose of performing different catalytic reactions as steam methane reforming (SMR) or methane dehydroaromatization (MDA) in a CMR. Targeted properties of the porous catalytic layers are listed: (a) high electronic conductivity; (b) redox stable under high steam content methane and coking resistant under atmospheres composed of dry methane, ethylene and aromatic vapours; and (c) high catalytic activity towards hydrogen activation. This work presents the development of different catalytic coatings based on LSC materials compatibles with LWO/LSC. H<sub>2</sub> permeation measurements have been performed by using 60/40-LWO/LSC membranes with the developed catalytic coatings. H<sub>2</sub> flux has been studied as a function of the temperature, of the H<sub>2</sub> concentration in the feed and hydration conditions of the membrane. For the best membrane, H<sub>2</sub> permeation measurements under CH<sub>4</sub> containing stream have been accomplished. Finally, stability tests under high steam content methane have been performed and the integrity of the samples has been evaluated by XRD and SEM.

## 2. Experimental

60/40-LWO/LSC (60:40 vol%) composite was prepared by mixing the corresponding amounts of LWO (provided by Cerprotech (NO) and calcined at 800 °C) and LSC (provided by Praxair (US) and calcined at 900 °C) and both materials were ball-milled together for 24 hours.

LSC based materials (employed as catalytic layers) as powders were synthesized by using the citrate reaction route [27] with a final calcination temperature of 900 and 1000 °C. The following LSC based materials were synthesized: La<sub>0.87</sub>Sr<sub>0.13</sub>CrO<sub>3-δ</sub> (LSC), La<sub>0.75</sub>Ce<sub>0.1</sub>Sr<sub>0.15</sub>CrO<sub>3-δ</sub> (LCeSC), La<sub>0.85</sub>Sr<sub>0.15</sub>Cr<sub>0.8</sub>Ni<sub>0.2</sub>O<sub>3-δ</sub> (LSCN) and La<sub>0.75</sub>Ce<sub>0.1</sub>Sr<sub>0.15</sub>Cr<sub>0.95</sub>Ru<sub>0.05</sub>O<sub>3-δ</sub> (LCeSCR).

Crystalline phases were identified by X-ray diffraction (XRD) performed in a CubiX FAST equipment using CuK $\alpha_{1,2}$  radiation and an X'Celerator detector in Bragg-Brentano geometry in the 2 $\theta$  range from 20 to 70°. XRD patterns were analyzed using X'PertHighscore Plus software (PANalytical).

Composite membranes used in H<sub>2</sub> permeation measurements consisted of a gastight disc with 15 mm diameter. Membranes were prepared by uniaxially pressing at 72 MPa of the mixtures before sintering at 1550 °C for 6 h in air.

Catalytic layers made of LSC based materials were obtained by screen-printing the inks on both sides of 60/40-LWO/LSC membranes. Inks were made by mixing the milled powders with a solution of ethylcellulose in terpineol (6%-wt.) and subsequently refined using a three roller mill (Exakt). Pt conducting paste was provided by MaTeck (Germany).

Six different coatings were prepared: (a) Pt (reference), (b) LSC, (c) LCeSC, (d) LSCN, (e) LCeSCR and (f) LCeSC infiltrated with Ni, in order to promote the surface reactions. Ni infiltration was made by following the procedure explained elsewhere [27] and using 5 M water solution of Ni nitrate. Firing temperature of screen-printed membranes was 1150 °C for 2 h.

Permeation measurements were performed on a double chamber quartz reactor following the procedure describe elsewhere [28, 29]. A mixture of H<sub>2</sub>-He (100 mL·min<sup>-1</sup>) was used as feed gas whereas Ar was employed as sweep gas (150 mL·min<sup>-1</sup>). The H<sub>2</sub> content in the permeate side was analyzed using micro-GC Varian CP-4900 equipped with Molsieve5A and PoraPlot-Q glass capillary modules. Sealing was obtained using silver rings and applying a spring load. Appropriate sealing was confirmed by continuously monitoring the He concentration in the permeate stream. An acceptable sealing was considered when the helium concentration was lower than 5% of the H<sub>2</sub> permeated. Real H<sub>2</sub> permeation was then calculated by subtracting the He to the total H<sub>2</sub> flow observed [30].

Permeation measurements were accomplished under four hydration degree configurations: C1, dry atmosphere in both sides of the membrane (feed and permeate side); C2, feed side humidified (pH<sub>2</sub>O=0.03 atm); C3, both membrane sides humidified (pH<sub>2</sub>O=0.03 atm) and C4, sweep side humidified (pH<sub>2</sub>O=0.03 atm). Permeation was also performed by using 30% CH<sub>4</sub>, 50% H<sub>2</sub> and 20% He as feed, in order to check the H<sub>2</sub> flux under CH<sub>4</sub> containing atmospheres.

60-LWO/LSC (without catalytic layer), LCeSCRu and LCeSC-Ni samples were subsequently treated under an atmosphere composed by 50 % CH<sub>4</sub> and 50% H<sub>2</sub>O, at 3 bar and 700 °C for 24 hours.

The microstructure of the catalytic layers and membranes was investigated using field emission scanning electron microscopy (FE-SEM) (Zeiss Ultra 55) and elemental analysis was carried out with energy-dispersive X-ray spectroscopy (EDS) (INCA, Oxford). The integrity of the samples was also checked by XRD.

### **3. Results**

#### **3.1. Synthesis of LSC based materials**

Formula of the synthesized compounds based on LSC, their abbreviation and the corresponding calcination temperature are listed in Table 1. Room temperature XRD patterns of the developed LSC based materials as powders listed in Table 1 are shown in Figure 1. The predominant crystalline phase corresponds to the orthorhombic perovskite [31], however some minor peaks ascribed to SrCrO<sub>4</sub> and CeO<sub>2</sub> impurities can be also observed. Nevertheless, these impurities

disappear at higher calcination temperatures,  $T > 1050$  °C [32], where no secondary phases are detected as can be observed in Figure 7.

Compounds	Nomenclature	Calcination temperature of the powder (°C)
$\text{La}_{0.87}\text{Sr}_{0.13}\text{CrO}_{3-\delta}$	LSC	900
$\text{La}_{0.75}\text{Ce}_{0.1}\text{Sr}_{0.15}\text{CrO}_{3-\delta}$	LCeSC	900
$\text{La}_{0.75}\text{Ce}_{0.1}\text{Sr}_{0.15}\text{Cr}_{0.95}\text{Ru}_{0.05}\text{O}_{3-\delta}$	LCeSCR	1000
$\text{La}_{0.85}\text{Sr}_{0.15}\text{Cr}_{0.8}\text{Ni}_{0.2}\text{O}_{3-\delta}$	LSCN	900

Table 1: Stoichiometry, nomenclature and calcination temperature of LSC based compounds developed for catalytic coatings.

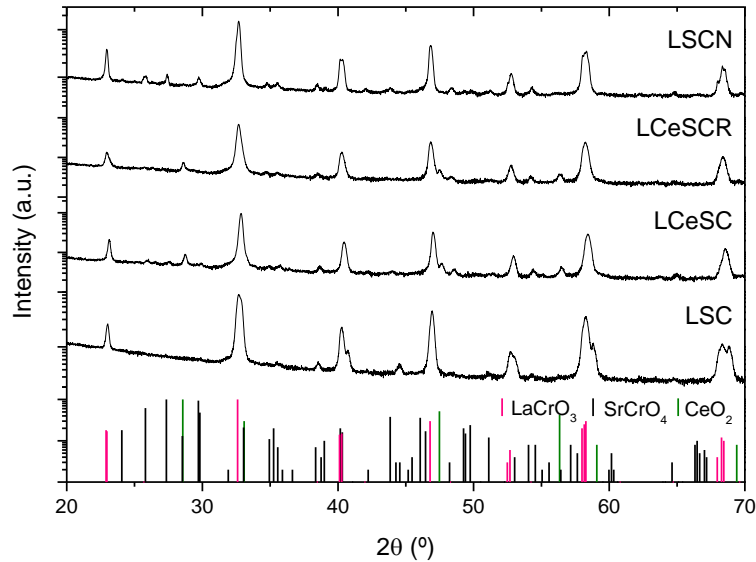


Figure 1: XRD patterns (y axis in  $\log$  scale) of the LSC calcined powders. Reference patterns of  $\text{SrCrO}_4$ ,  $\text{LaCrO}_3$  and  $\text{CeO}_2$  have been depicted for comparison (bottom).

## 3.2. Hydrogen permeation

### 3.2.1. Pt catalytic coating

The 60/40-LWO/LSC composition was selected due to the significant  $\text{H}_2$  permeation that presents, higher than the reported for 20/80-LWO/LSC and 50/50-LWO/LSC [16].  $\text{H}_2$  fluxes for the three composites (expressed as  $\text{mL}\cdot\text{min}^{-1}\cdot\text{cm}^{-1}$  in order to disregard the effect of the thickness) are plotted in Figure 2a as a function of temperature under C3 conditions. Note that the three membranes were coated with Pt ink on both sides of the membrane.  $\text{H}_2$  flux obtained for 60/40-LWO/LSC is 1.1 and 3.9 times higher than 50/50-LWO/LSC and 20/80-LWO/LSC, respectively.

Permeation of 60/40-LWO/LSC coated with Pt was evaluated as a function of the temperature under four different hydration conditions: (C1) both sides of the membrane dry, (C2) feed side humidified, (C3) both sides of the membrane humidified and (C4) only sweep side humidified. Humidified gas streams contains 3% of water ( $p_{\text{H}_2\text{O}}=0.03$  atm). The  $\text{H}_2$  fluxes obtained are depicted in Figure 2b. Different behaviours can be distinguished depending on the gas hydration configuration, as it was previously observed for 50/50-LWO/LSC.  $\text{H}_2$  flux is very low under C1 as corresponds to the deficiency of protonic charge carriers in the oxide under dry conditions.  $\text{H}_2$  permeation increases when  $\text{H}_2$  feed side is humidified (C2) due to the hydration of the membrane and the subsequently increase of proton incorporation. Under C3 and C4, water splitting in the sweep side originated from the oxygen ion transport from the sweep side to the feed side contributes to the total  $\text{H}_2$  flux. In fact, when both sides are humidified, C3, the  $\text{H}_2$  flux increases reaching values up to  $0.22 \text{ mL}\cdot\text{min}^{-1}\cdot\text{cm}^{-2}$ . This rise is related to the higher proton transport and stems from the enhanced hydration degree of the oxide which provokes an increase in the proton concentration and thus in the proton. A contribution of 50% proton transport-50% water splitting has been reported for 50/50-LWO/LSC at  $700^\circ\text{C}$  under similar conditions using deuterium-labelled tracers [24]. For that reason together with the prevailing proton conductivity of LWO [33] in this range of temperature, at least a contribution of 50% proton transport is expected for the studied composite material.

On the other hand, when only the sweep side is humidified,  $\text{H}_2$  flux decreases as compared with the previous condition. This drop is related to the lower degree of hydration of the membrane which causes the decrease of the proton transport. Conversely, in this configuration, the  $p_{\text{O}_2}$  gradient is slightly higher than in the previous one, resulting in an increase in the  $\text{H}_2$  flux produced via water splitting. The point that  $\text{H}_2$  flux in C4 is lower than in C3 indicates a prevailing proton transport in the material within the studied temperature range. This behaviour is in line with the transference number of LWO [33], i.e., this effect becomes progressively more important with decreasing temperatures and protons become the prevailing carriers at temperatures below  $700^\circ\text{C}$ .

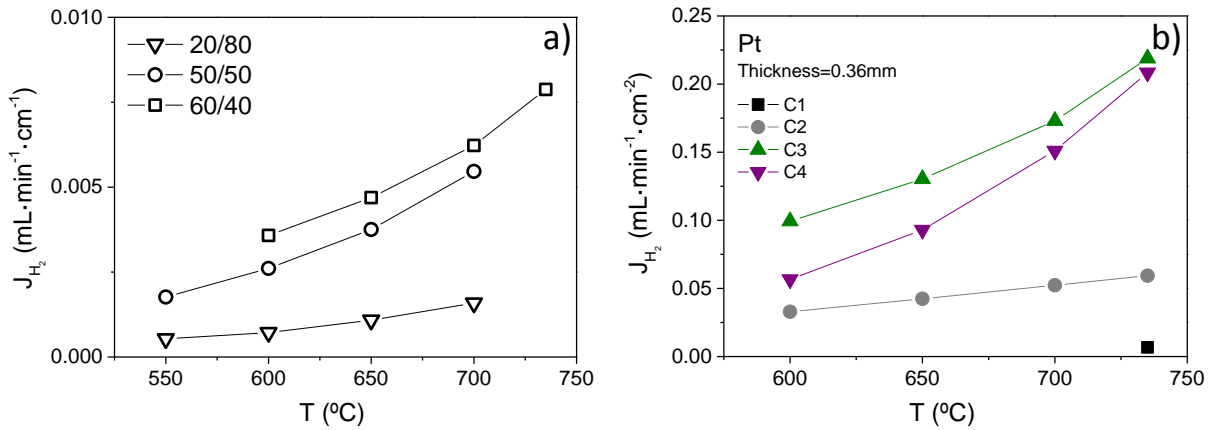


Figure 2: H<sub>2</sub> flux (permeability) as a function of temperature for 20/80, 50/50 and 60/40-LWO/LSC with a Pt coating under C3 configuration expressed as mL·min<sup>-1</sup>·cm<sup>-1</sup> (b) H<sub>2</sub> flux (expressed as mL·min<sup>-1</sup>·cm<sup>-2</sup>) as a function of temperature for 60/40-LWO/LSC under C1, C2, C3 and C4 configurations.

### 3.2.2. LSC based catalytic coatings

The H<sub>2</sub> permeation was studied for different 60/40-LWO/LSC membranes activated using five different porous catalytic coatings on both sides of the membrane: (i) 20 μm layer of LSC, (ii) 20 μm layer of LCeSC, (iii) 20 μm layer of LCeSCR, (iv) 20 μm layer of LSCN and (v) 20 μm layer of LCeSC infiltrated with Ni (LCeSC-Ni). All deposited LSC layers were sintered in air at 1150 °C. This sintering temperature was previously optimized to reach proper electrochemical performance for LSCN when tested as proton conducting fuel cell anode on LWO electrolytes [32].

Figure 3 shows the H<sub>2</sub> permeation fluxes as a function of the temperature for the membranes coated with LSC (a), LCeSC (b), LCeSCR (c), LSCN (d) and LCeSC-Ni (e). Only the membranes coated with LSC and LCeSC-Ni present similar behavior depending on the hydration configuration as Pt coated membrane, i.e. H<sub>2</sub> flux in C3 is higher than in C4. This indicates that the degree of hydrogen flux vs hydrogen produced by water splitting is influenced by the catalytic layer. Both LCeSCR and LCeSC present an increased catalytic activity toward O<sub>2</sub> exchange that gives rise to a higher contribution of the H<sub>2</sub> produced by water splitting as compared to H<sub>2</sub> permeation. LSCN presents an unexpected behaviour; one would expect the same behaviour as LCeSC-Ni, maybe with lower catalytic activity due to the lower Ni concentration.

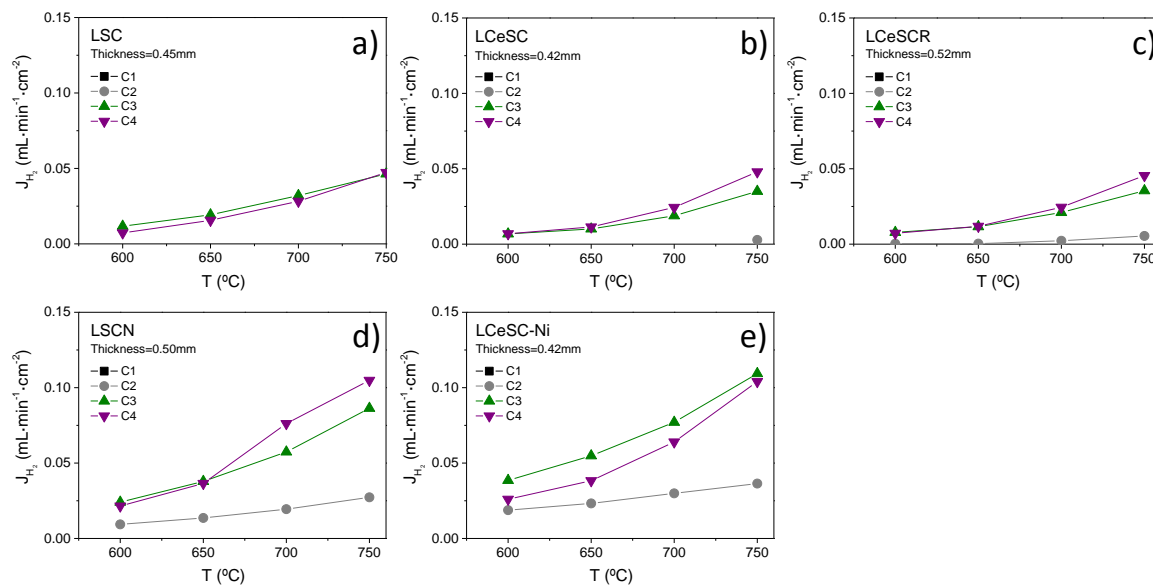


Figure 3: H<sub>2</sub> flux as function of temperature for 60/40-LWO/LSC with different activation catalytic layers: LSC (a), LSCN (b), LCeSCR (c), LCeSC (d) and LCeSC-Ni (e) in four different hydration degree configurations: C2, C3 and C4.

A comparison of the H<sub>2</sub> fluxes (expressed as mL·min<sup>-1</sup>·cm<sup>-1</sup>, in order to neglect the thickness influence) obtained for the five membranes with different catalytic layers and Pt coated membrane is depicted in Figure 4 for C2 (a), C3 (b) and C4 (c) conditions. Pt activated membrane presents the highest H<sub>2</sub> fluxes in the three evaluated conditions, followed by the LCeSC-Ni and LSCN coated membranes. Ni nanoparticles are formed on the LCeSC-Ni grain surface due to the reduction of the infiltrated Ni [34] whereas on LSCN they are formed from Ni reduction with subsequently precipitation on the grain surface [35]. The higher H<sub>2</sub> flux obtained with the Ni containing layers is ascribed to the active catalytic activity of Ni nanoparticles for the H<sub>2</sub>/O<sub>2</sub> bond breaking in addition with the high electronic conductivity of these compounds which allows the three-phase boundary area to be increased. In fact, the addition of Ni to LSC anodes has been reported to boost surface reaction processes, appearing at low frequencies in impedance spectra [27]. This improvement was higher (as in this work) when the Ni was infiltrated, ascribed to a better dispersion and higher surface coverage of Ni nanoparticles [27, 34]. However, under C4 condition, the values obtained with LSCN are slightly higher at the highest tested temperature and the cause of this effect remains unknown. At this point, one may speculate about the distinct activity of the Ni reaction sites in LSCN and Ni-infiltrated electrodes towards H<sub>2</sub> activation and water splitting. Specifically, the results for C4 (dry feed side) may suggest that the infiltrated Ni particles are more active towards water splitting than the particles from the LSCN.

On the other hand, H<sub>2</sub> fluxes obtained for the LSC, LCeSC and LCeSCR activated membranes present practically the same values, indicating a relatively low catalytic activity for H<sub>2</sub> and O<sub>2</sub> evolution/oxidation reactions [36]. Despite the higher total and *p*-type electronic conductivity that LCeSC possesses [34] and the relatively high catalytic activity of Ru [37] for hydrocarbon reforming and syngas conversion, these membranes exhibit a similar magnitude of the H<sub>2</sub> flux as the obtained using the LSC activated membrane. The low catalytic activity of LCeSCR could be related with the Ru concentration in the perovskite lattice, which turns out to be insufficient to form enough Ru<sup>0</sup> nanoparticles by precipitation on the grain surface and to reach a proper surface coverage of the LCeSCR backbone structure.

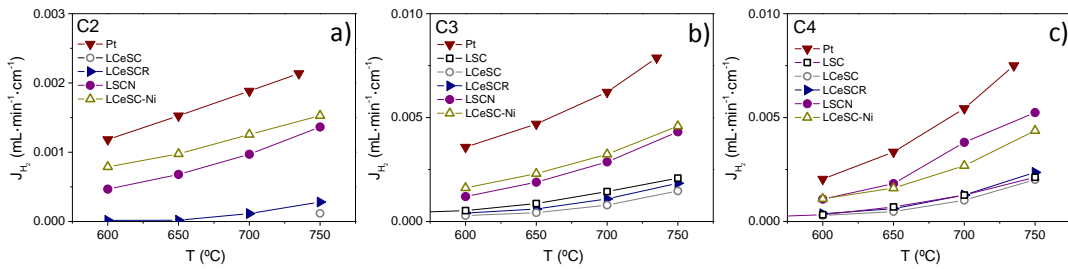


Figure 4: Comparison of the H<sub>2</sub> flux obtained for 60/40-LWO/LSC with the different activation catalytic layers under C2 (a), C3 (b) and C4 (c) hydration configurations. Note the distinct y-axis for (a)

### 3.3. Stability study

The stability and proton transport under CH<sub>4</sub> atmospheres was evaluated for LCeSC-Ni coated membrane. With this purpose, H<sub>2</sub> permeation measurements were performed at 750 °C during 5 hours feeding 30% CH<sub>4</sub>, 50% H<sub>2</sub> and 20% He and humidifying both sides of the membrane (C3) (note that the same specimen was used in all the measurements, without and with CH<sub>4</sub> in the feed). H<sub>2</sub> fluxes obtained by using 50% H<sub>2</sub>-50% He and 30% CH<sub>4</sub>-50% H<sub>2</sub>-20% He as feed gas are compared in Figure 5. H<sub>2</sub> flux obtained under CH<sub>4</sub> containing atmosphere remained unchanged for 6 hours which demonstrates the stability of the compound in these conditions. In addition, permeation values were higher than those obtained employing 50% H<sub>2</sub>-50% He as expected from the higher *p*H<sub>2</sub> gradient under CH<sub>4</sub>-containing stream, i.e., larger driving force for the separation.

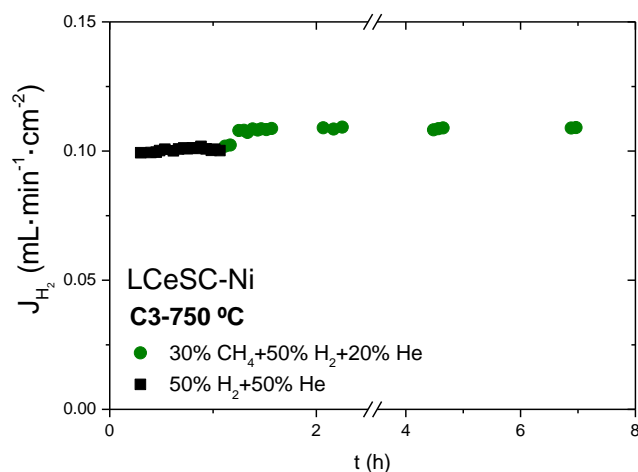


Figure 5: H<sub>2</sub> flux as a function of time for 60/40-LWO/LSC coated with LCeSC-Ni feeding 50% H<sub>2</sub> in He and a mixture composed by 30% CH<sub>4</sub>, 50% H<sub>2</sub> and 20% He at 750 °C.

The microstructure of the catalytic layers after the permeation measurements was checked by FE-SEM analysis. Images of the LCeSC (a), LCeSC-Ni (b) and LCeSCR (c) coated membranes (Figure 6) reveal that the integrity of the interface between catalytic layer and membrane is well-preserved. Figure 6 d-i shows the morphology of the catalytic layers. LCeSC presents a heterogeneous distribution of the particle size, ranging from 0.2 to 1 μm (Figure 6d,g). Ni nanoparticles fully cover the LCeSC-Ni grain surface as can be observed in Figure 6e,h. Higher magnification images of them could not be obtained due to the organic remains after permeation measurements that could be ascribed to the coke formation when CH<sub>4</sub> was used as feed. Finally, Ru nanoparticles were not detected in LCeSCR (Figure 6f,i), fact that can explain its lower catalytic activity.

After the permeation measurements, the stability under high steam content methane of the LCeSCRu and LCeSC-Ni coated membranes was evaluated by annealing under an atmosphere composed by 50% CH<sub>4</sub> and 50% H<sub>2</sub>O at 700 °C and 3 bars for 24 hours. These conditions are mimicking those encountered in steam methane reforming (SMR) reactors, which is an appealing application for high temperature hydrogen membrane. The integrity of the samples was checked by XRD before and after the treatment. The samples treated under the abovementioned conditions were the previous used membranes in permeation measurements. XRD patterns of these membranes before and after the treatment are displayed in Figure 7 where no secondary phases can be detected after the annealing. Furthermore, no reaction or interaction between metallic Ni nanoparticles and LWO can be observed, proving the compatibility between Ni/LWO under permeation conditions [38, 39]. This is indeed a crucial aspect since NiO and LWO are prone to react at temperatures above 900 °C under oxidizing conditions.

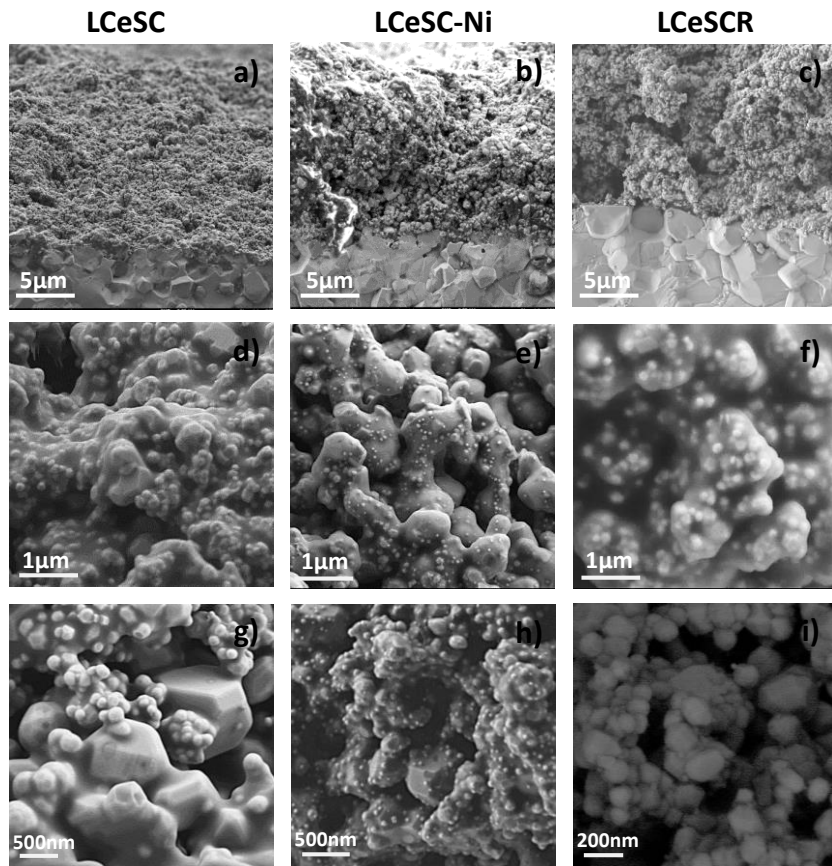


Figure 6: SEM analysis of the fractured cross-section of the studied membranes (a,b,c) and catalytic surface (d-i).

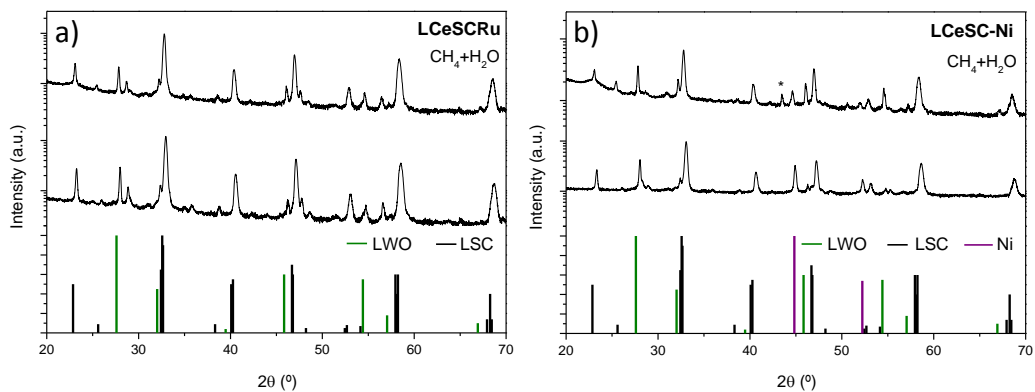


Figure 7: XRD patterns of the membranes coated with LCeSCRu (a) and LCeSC-Ni (b) after stability treatment (50% CH<sub>4</sub> and 50% H<sub>2</sub>O at 700 °C and 3 bars for 24 hours). \* corresponds to sample holder.

In order to check the integrity of the microstructure after the treatment under SMR conditions (50% CH<sub>4</sub> and 50% H<sub>2</sub>O at 700 °C), the samples were analyzed by FE-SEM and EDS analysis.

In Figure 8 the fracture cross-sections of LCeSC-Ni and LCeSCRu coated membranes are depicted. To the limit of the technique, the formation of secondary phases during the annealing is not detected. In addition, the membranes are totally dense after the treatment and the layers present good adhesion to the underneath membrane. Well dispersed Ni nanoparticles are detected in the layer LCeSC-Ni. On the other hand, no Ru was detected in the sample LCeSCRu and this fact is ascribed to the initial low concentration of Ru in the sample, which appears to be responsible for the low catalytic activity observed for this sample in the H<sub>2</sub> permeation measurements.

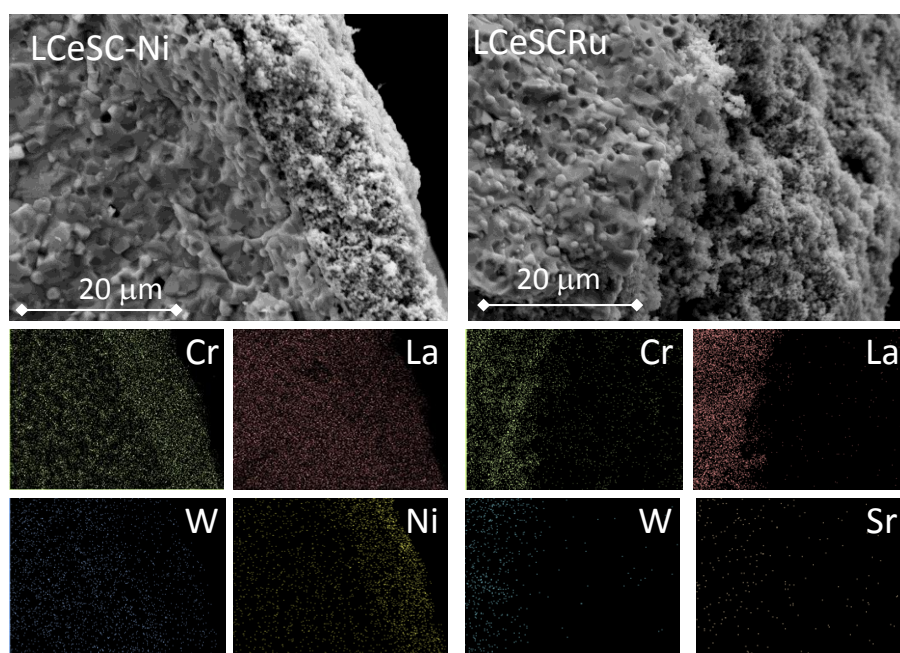


Figure 8: SEM analysis of the fractured cross-section of the LCeSC-Ni and LCeSCRu coated membranes after stability treatment (50% CH<sub>4</sub> and 50% H<sub>2</sub>O at 700 °C and 3 bars for 24 hours) and EDS analysis.

#### 4. Conclusions

Different catalytic layers for H<sub>2</sub> evolution have been developed for the surface functionalization of ceramic hydrogen-separation membranes based on LWO/LSC composites, specifically for application in steam methane reforming and MDA using catalytic membrane reactors.

LSC based materials were selected with this purpose for the compatibility with the membrane materials and the promising electrochemical properties as fuel cell anodes. Five layers were deposited and the highest H<sub>2</sub> flux was obtained by using LCeSC-Ni coated membrane due to the important catalytic activity of the Ni nanoparticles to H<sub>2</sub> dissociation, oxidation and surface diffusion of H species. Furthermore, stability of the H<sub>2</sub> permeation by feeding CH<sub>4</sub> was confirmed. In addition, stability under an atmosphere composed by 50% CH<sub>4</sub> and 50% H<sub>2</sub>O at

700 °C and 3 bars for LCeSCR and LCeSC-Ni coated membranes was demonstrated at least for 24 hours. Due to the high H<sub>2</sub> flux obtained and the stability under CH<sub>4</sub> and high steam concentration, LWO/LSC composites and LSC based materials are presented as promising membranes and catalytic layers for their application in catalytic membrane reactors.

### Acknowledgements

Financial support by the Spanish Government (Grants ENE2014-57651-R, CSD-2009-0050 and SEV-2012-0267) and CoorsTek Membrane Sciences is kindly acknowledged. The authors are indebted to M. Fabuel for sample preparation. The support of the Servicio de Microscopía Electrónica of the Universidad Politécnica de Valencia is also acknowledged.

### References

- [1] L. Barelli, G. Bidini, F. Gallorini, S. Servili, Hydrogen production through sorption-enhanced steam methane reforming and membrane technology: A review, *Energy*, 33 (2008) 554-70.
- [2] M.C. Alvarez-Galvan, N. Mota, M. Ojeda, S. Rojas, R.M. Navarro, J.L.G. Fierro, Direct methane conversion routes to chemicals and fuels, *Catalysis Today*, 171 (2011) 15-23.
- [3] A.M. Adris, C.J. Lim, J.R. Grace, The fluidized-bed membrane reactor for steam methane reforming: model verification and parametric study, *Chemical Engineering Science*, 52 (1997) 1609-22.
- [4] L. Li, R.W. Borry, E. Iglesia, Design and optimization of catalysts and membrane reactors for the non-oxidative conversion of methane, *Chemical Engineering Science*, 57 (2002) 4595-604.
- [5] X. Dong, W. Jin, N. Xu, K. Li, Dense ceramic catalytic membranes and membrane reactors for energy and environmental applications, *Chemical Communications*, 47 (2011) 10886-902.
- [6] G. Saracco, H.W.J.P. Neomagus, G.F. Versteeg, W.P.M.v. Swaij, High-temperature membrane reactors: potential and problems, *Chemical Engineering Science*, 54 (1999) 1997-2017.
- [7] W. Meulenberg, M. Ivanova, H. Buchkremer, D. Stöver, J.S. Alfaro, S. Escolástico, CO<sub>2</sub>-tolerant, mixed conductive oxide and use thereof for hydrogen separation, *International Patent WO 2012/010386 A1*, 26 January, (2012).
- [8] E. Rebollo, C. Mortalo, S. Escolastico, S. Boldrini, S. Barison, J.M. Serra, M. Fabrizio, Exceptional hydrogen permeation of all-ceramic composite robust membranes based on BaCe<sub>0.65</sub>Zr<sub>0.20</sub>Y<sub>0.15</sub>O<sub>3</sub>-[small delta] and Y- or Gd-doped ceria, *Energy & Environmental Science*, (2015).
- [9] J. Li, H. Yoon, T.-K. Oh, E.D. Wachsman, High temperature SrCe<sub>0.9</sub>Eu<sub>0.1</sub>O<sub>3-δ</sub> proton conducting membrane reactor for H<sub>2</sub> production using the water-gas shift reaction, *Applied Catalysis B: Environmental*, 92 (2009) 234-39.
- [10] J. Li, H. Yoon, T.-K. Oh, E.D. Wachsman, SrCe<sub>0.7</sub>Zr<sub>0.2</sub>Eu<sub>0.1</sub>O<sub>3</sub>-based hydrogen transport water gas shift reactor, *International Journal of Hydrogen Energy*, 37 (2012) 16006-12.

- [11] H. Kim, B. Kim, J. Lee, K. Ahn, H.-R. Kim, K.J. Yoon, B.-K. Kim, Y.W. Cho, H.-W. Lee, J.-H. Lee, Microstructural adjustment of Ni–BaCe<sub>0.9</sub>Y<sub>0.1</sub>O<sub>3-δ</sub> cermet membrane for improved hydrogen permeation, *Ceramics International*, 40 (2014) 4117-26.
- [12] C. Zuo, S.E. Dorris, U. Balachandran, M. Liu, Effect of Zr-Doping on the Chemical Stability and Hydrogen Permeation of the Ni–BaCe<sub>0.8</sub>Y<sub>0.2</sub>O<sub>3-α</sub> Mixed Protonic–Electronic Conductor, *Chemistry of Materials*, 18 (2006) 4647-50.
- [13] Y. Wei, J. Xue, W. Fang, Y. Chen, H. Wang, J. Caro, Enhanced stability of Zr-doped Ba(CeTb)O<sub>3</sub>-[small delta]-Ni cermet membrane for hydrogen separation, *Chemical Communications*, 51 (2015) 11619-21.
- [14] E. Rebollo, C. Mortalo, S. Escolastico, S. Boldrini, S. Barison, J.M. Serra, M. Fabrizio, Exceptional hydrogen permeation of all-ceramic composite robust membranes based on BaCe<sub>0.65</sub>Zr<sub>0.20</sub>Y<sub>0.15</sub>O<sub>3-delta</sub> and Y- or Gd-doped ceria, *Energy & Environmental Science*, 8 (2015) 3675-86.
- [15] W.A. Rosensteel, S. Ricote, N.P. Sullivan, Hydrogen permeation through dense BaCe<sub>0.8</sub>Y<sub>0.2</sub>O<sub>3-δ</sub> - Ce<sub>0.8</sub>Y<sub>0.2</sub>O<sub>2-δ</sub> composite-ceramic hydrogen separation membranes, *International Journal of Hydrogen Energy*, 41 (2016) 2598-606.
- [16] S. Escolástico, C. Solís, C. Kjølseth, J.M. Serra, Outstanding hydrogen permeation through CO<sub>2</sub>-stable dual-phase ceramic membranes, *Energy and Environmental Science*, 7 (2014) 3736-46.
- [17] J.M. Polfus, W. Xing, M.F. Sunding, S.M. Hanetho, P.I. Dahl, Y. Larring, M.-L. Fontaine, R. Bredesen, Doping strategies for increased oxygen permeability of CaTiO<sub>3</sub> based membranes, *Journal of Membrane Science*, 482 (2015) 137-43.
- [18] F.M. Figueiredo, V.V. Kharton, A.P. Viskup, J.R. Frade, Surface enhanced oxygen permeation in CaTi<sub>1-x</sub>Fe<sub>x</sub>O<sub>3-δ</sub> ceramic membranes, *Journal of Membrane Science*, 236 (2004) 73-80.
- [19] Y. Wang, H. Hao, J. Jia, D. Yang, X. Hu, Improving the oxygen permeability of Ba<sub>0.5</sub>Sr<sub>0.5</sub>Co<sub>0.8</sub>Fe<sub>0.2</sub>O<sub>3-δ</sub> membranes by a surface-coating layer of GdBaCo<sub>2</sub>O<sub>5+δ</sub>, *Journal of the European Ceramic Society*, 28 (2008) 3125-30.
- [20] X. Tan, Z. Wang, H. Liu, S. Liu, Enhancement of oxygen permeation through La<sub>0.6</sub>Sr<sub>0.4</sub>Co<sub>0.2</sub>Fe<sub>0.8</sub>O<sub>3-δ</sub> hollow fibre membranes by surface modifications, *Journal of Membrane Science*, 324 (2008) 128-35.
- [21] M.P. Lobera, S. Escolastico, J. Garcia-Fayos, J.M. Serra, Ethylene Production by ODHE in Catalytically Modified Ba<sub>0.5</sub>Sr<sub>0.5</sub>Co<sub>0.8</sub>Fe<sub>0.2</sub>O<sub>3-delta</sub> Membrane Reactors, *ChemSusChem*, 5 (2012) 1587-96.
- [22] G.C. Mather, D. Poulidi, A. Thursfield, M.J. Pascual, J.R. Jurado, I.S. Metcalfe, Hydrogen-permeation characteristics of a SrCeO<sub>3</sub>-based ceramic separation membrane: Thermal, ageing and surface-modification effects, *Solid State Ionics*, 181 (2010) 230-35.
- [23] S. Escolastico, S. Somacescu, J.M. Serra, Solid State Transport and Hydrogen Permeation in the System Nd<sub>5.5</sub>W<sub>1-x</sub>RexO<sub>11.25-delta</sub>, *Chemistry of Materials*, 26 (2014) 982-92.
- [24] S. Escolastico, C. Solis, C. Kjolseth, J.M. Serra, Outstanding hydrogen permeation through CO<sub>2</sub>-stable dual-phase ceramic membranes, *Energy & Environmental Science*, 7 (2014) 3736-46.
- [25] J.M. Polfus, W. Xing, M.-L. Fontaine, C. Denonville, P.P. Henriksen, R. Bredesen, Hydrogen separation membranes based on dense ceramic composites in the La<sub>27</sub>W<sub>5</sub>O<sub>55.5</sub>–LaCrO<sub>3</sub> system, *Journal of Membrane Science*, 479 (2015) 39-45.

- [26] J. Song, J. Kang, X. Tan, B. Meng, S. Liu, Proton conducting perovskite hollow fibre membranes with surface catalytic modification for enhanced hydrogen separation, *Journal of the European Ceramic Society*, 36 (2016) 1669-77.
- [27] C. Solís, M. Balaguer, F. Bozza, N. Bonanos, J.M. Serra, Catalytic surface promotion of highly active  $\text{La}_{0.85}\text{Sr}_{0.15}\text{Cr}_{0.8}\text{Ni}_{0.2}\text{O}_{3-\delta}$  anodes for  $\text{La}_{5.6}\text{WO}_{11.4-\delta}$  based proton conducting fuel cells, *Applied Catalysis B: Environmental*, 147 (2014) 203-07.
- [28] S. Escolastico, M. Schroeder, J. Serra, Optimization of the Mixed Proton-Electronic Conducting Materials based on the  $(\text{Nd}_{5/6}\text{Ln}_{1/6})_{5.5}\text{WO}_{11.25-\delta}$ , *Journal of Materials Chemistry A*, 26 (2014) 982-92.
- [29] S. Escolastico, S. Somacescu, J.M. Serra, Tailoring mixed ionic-electronic conduction in  $\text{H}_2$  permeable membranes based on the system  $\text{Nd}_{5.5}\text{W}_{1-x}\text{MoxO}_{11.25-\delta}$ , *Journal of Materials Chemistry A*, 3 (2015) 719-31.
- [30] J. Song, L. Li, X. Tan, K. Li,  $\text{BaCe}_{0.85}\text{Tb}_{0.05}\text{Co}_{0.1}\text{O}_{3-\delta}$  perovskite hollow fibre membranes for hydrogen/oxygen permeation, *International Journal of Hydrogen Energy*, 38 (2013) 7904-12.
- [31] B.I. Lee, R.K. Gupta, C.M. Whang, Effects of solvent and chelating agent on synthesis of solid oxide fuel cell perovskite,  $\text{La}_{0.8}\text{Sr}_{0.2}\text{CrO}_{3-\delta}$ , *Materials Research Bulletin*, 43 (2008) 207-21.
- [32] C. Solís, L. Navarrete, M. Balaguer, J.M. Serra, Development and understanding of  $\text{La}_{0.85}\text{Sr}_{0.15}\text{Cr}_{1-x}\text{Ni}_x\text{O}_{3-\delta}$  anodes for  $\text{La}_{5.6}\text{WO}_{11.4-\delta}$ -based Proton Conducting Solid Oxide Fuel Cells, *Journal of Power Sources*, 258 (2014) 98-107.
- [33] R. Haugsrud, C. Kjølleth, Effects of protons and acceptor substitution on the electrical conductivity of  $\text{La}_6\text{WO}_{12}$ , *Journal of Physics and Chemistry of Solids*, 69 (2008) 1758-65.
- [34] M. Balaguer, C. Solís, F. Bozza, N. Bonanos, J.M. Serra, High performance anodes with tailored catalytic properties for  $\text{La}_{5.6}\text{WO}_{11.4-\delta}$  based proton conducting fuel cells, *Journal of Materials Chemistry A*, 1 (2013) 3004-07.
- [35] V.B. Vert, F.V. Melo, L. Navarrete, J.M. Serra, Redox stability and electrochemical study of nickel doped chromites as anodes for  $\text{H}_2/\text{CH}_4$ -fueled solid oxide fuel cells, *Applied Catalysis B: Environmental*, 115-116 (2012) 346-56.
- [36] J. Greeley, N.M. Markovic, The road from animal electricity to green energy: combining experiment and theory in electrocatalysis, *Energy & Environmental Science*, 5 (2012) 9246-56.
- [37] J. Rossmeisl, W.G. Bessler, Trends in catalytic activity for SOFC anode materials, *Solid State Ionics*, 178 (2008) 1694-700.
- [38] S.J. Song, E.D. Wachsman, J. Rhodes, H.S. Yoon, K.H. Lee, G. Zhang, S.E. Dorris, U. Balachandran, Hydrogen permeability and effect of microstructure on mixed protonic-electronic conducting Eu-doped strontium cerate, *J Mater Sci*, 40 (2005) 4061-66.
- [39] C. Solís, V.B. Vert, M. Balaguer, S. Escolástico, S. Roitsch, J.M. Serra, Mixed proton-electron conducting chromite electrocatalysts as anode materials for LWO-based solid oxide fuel cells, *ChemSusChem*, 5 (2012) 2155-58.